minerals

MDPI

Article

REE Distribution in Lake Van Stromatolites: Detrital vs. Authigenic Signature

Bilge Sasmaz [1,2], Marianna Cangemi [3,4,*], Ygor Oliveri [5] and Ahmet Sasmaz [1]

[1] Department of Geological Engineering, Fırat University, 23119 Elazig, Turkey; sasmazbilge1@gmail.com (B.S.); asasmaz@firat.edu.tr (A.S.)
[2] Department of Earth and Atmospheric Sciences, University of Houston, Houston, TX 77204, USA
[3] Istituto Nazionale di Geofisica e Vulcanologia, Sezione di Catania-Osservatorio Etneo, Piazza Roma 2, 95125 Catania, Italy
[4] DiSTeM, University of Palermo, 90100 Palermo, Italy
[5] Istituto Nazionale di Geofisica e Vulcanologia, Sezione di Palermo, via Ugo La Malfa 153, 90146 Palermo, Italy; ygor.oliveri@ingv.it
* Correspondence: marianna.cangemi@ingv.it

Abstract

Lake Van (Eastern Turkey), the world's largest soda lake, represents a unique geochemical environment characterized by high alkalinity (pH about 9.7) and a complex hydrochemistry, driven by deep hydrothermal input and extreme evaporative processes. This article evaluates mineralogy, minor elements, and Rare Earth Element (REE) geochemistry of coastal stromatolites from 11 sites, to discriminate between endogenous chemical signals and terrigenous contamination. Results identify two distinct lithological groups: a chemically pure authigenic end-member ($CaCO_3$ > 85%), overprinted by a significant siliciclastic detrital contribution, rich in SiO_2, Al_2O_3, and Fe_2O_3. Authigenic samples successfully preserve the primary hydrothermal signature, exhibiting marked Heavy Rare Earth Element (HREE) enrichment and superchondritic Y/Ho ratios (=35), inherited from the stability of dissolved dicarbonate complexes, such as $[REE(CO_3)_2]^-$, which favor HREE solubility and uptake into the carbonate lattice. Conversely, the significant detrital contribution is highlighted by a robust correlation between REE and lithogenic proxies (Al-Si-Fe). Furthermore, the non-CHARAC behavior observed in Y/Ho and Zr/Hf twin pairs effectively distinguishes biogenic-chemical precipitation from detrital inputs. These results highlight the effectiveness of REE geochemistry as a proxy to filter out lithogenic overprints and accurately isolate the primary hydrochemical record of carbonate stromatolites.

Keywords: stromatolites; Lake Van; rare earth elements; Y/Ho and Zr/Hf twin pairs

Check for updates

Academic Editor: Pierpaolo Zuddas

Received: 31 January 2026
Revised: 17 February 2026
Accepted: 20 February 2026
Published: 23 February 2026

Copyright: © 2026 by the authors. Licensee MDPI, Basel, Switzerland. This article is an open access article distributed under the terms and conditions of the Creative Commons Attribution (CC BY) license.

1. Introduction

Stromatolites represent one of the most enduring and significant biological signatures in Earth's geological record. Defined as organo-sedimentary structures produced by the sediment-trapping, binding, and precipitating activities of microbial communities, primarily cyanobacteria, these formations provide a unique window into the early evolution of life and the environmental conditions of the Archean and Proterozoic eons [1–10].

The formation of these structures is now understood as a sophisticated interplay between microbial metabolism, carbonate chemistry, and specific environmental settings [11]. This "geobiological" perspective shifts the focus from purely morphological descriptions to a multidisciplinary approach that includes: (i) microbial diversity, moving beyond

cyanobacteria to investigate the roles of heterotrophic bacteria and archaea in the lithification process [12,13]; (ii) mineralization pathways, understanding the "alkalinity engine" and how metabolic activities facilitate the precipitation of calcium carbonate within the extracellular polymeric substances (EPS) matrix [14,15]; (iii) environmental proxies, using stromatolites as archives for Re-Os geochronology, stable isotope geochemistry, and paleo-oceanographic reconstructions [16,17].

Despite their decline in abundance following the "Cambrian explosion", often attributed to the rise of grazing metazoans [18], modern analogues in hypersaline lagoons and open-marine environments continue to offer invaluable insights [19]. By bridging the gap between ancient fossil records and contemporary microbial processes, we can better decipher the co-evolution of the biosphere and the geosphere.

A significant case study in modern geobiology is represented by Lake Van (Eastern Anatolia, Turkey), the world's largest soda lake. The stromatolites of Lake Van are renowned for their massive dimensions, forming towers that can reach up to 40 m in height. Unlike many marine stromatolites, these structures develop in an environment characterized by extreme alkalinity (pH ~9.7) and high salinity, which deeply influences the mineralization processes [20].

Recent literature highlights how the formation of Lake Van stromatolites is driven by a combination of: (i) mixing zones, where the precipitation of calcium carbonate is often triggered by the mixing of calcium-rich groundwater combined with the highly alkaline, carbonate-rich lake waters leading to significant carbonate oversaturation [21]; (ii) biological modulation, where abiotic factors play a primary role in the initial precipitation, and microbial mats, consisting of cyanobacteria and diverse heterotrophic consortia, stabilize these structures and influence their internal fabrics through the production of extracellular polymeric substances (EPS) [22,23]; (iii) environmental archives: these stromatolites serve as high-resolution archives for Late Quaternary climate changes and lake-level fluctuations, offering a continental perspective that complements the marine records typically discussed in geobiological studies [24]; (iv) isotopic and chemical signatures: stable isotope analyses of carbon and oxygen indicate that carbonate precipitation is governed primarily by inorganic equilibria [10]. Isotopic discrepancies observed in several samples and SEM observations of biogenic detritus, associated with authigenic carbonates, suggest that biological processes influence or modulate the dominant inorganic precipitation.

The aim of this study is to understand how the distribution of REE on stromatolites growing around the shoreline of Lake Van can be influenced by environmental parameters.

2. Study Area

Lake Van is the world's largest soda lake, with an area of 3712 km^2, and a maximum water depth of 451 m; it is located on the East Anatolian Plateau in eastern Turkey, at an altitude of 1648 m asl (Figure 1a). Subaerial and submerged stromatolites are common topographic features of the lake, and occur as swarms of column or tree-like buildups (Figure 1b). The basin is a tectonic depression formed by the collision of the Arabian and Eurasian plates, subsequently dammed by volcanic eruptions from Mount Nemrut during the Late Pleistocene. The lake catchment is geologically diverse, composed of Quaternary volcanic and Lower Miocene marine carbonates in the west and north, marbles and other metasedimentary rocks of the Bitlis Massif in the south, and Pliocene sedimentary rocks in the east [25]. Heat flow data suggest the presence of a magmatic body beneath the lake, possibly related to Nemrut Volcano, sustaining the input of CO_2 into its waters, whose chemistry is seasonally modulated by evaporitic conditions [10,26].

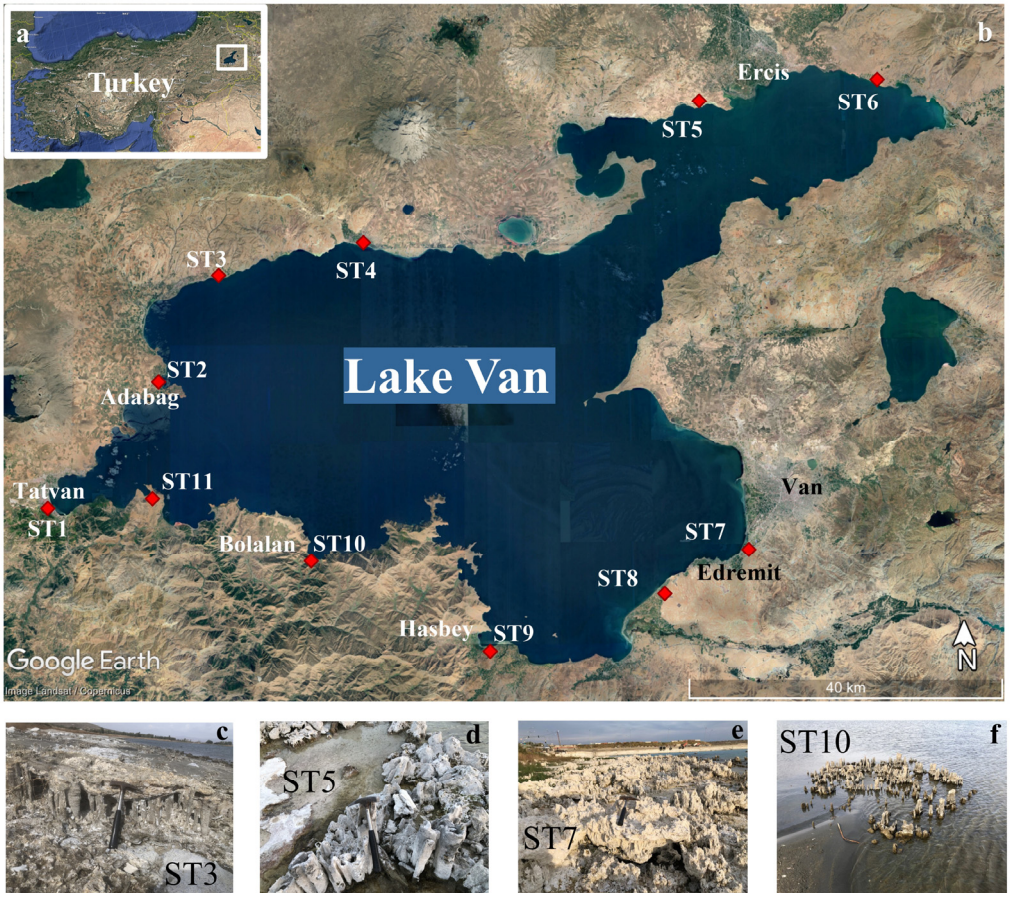


Figure 1. Map of Turkey (**a**) and location (**b**) of sampling points. Pictures close to ST3 (**c**), ST5 (**d**), ST7 (**e**), and ST10 (**f**).

The Van region is characterized by a continental climate, with cold and wet winters and warm and dry summers, where surface water temperatures fluctuate between 21 and 25 °C in summer and 2 and 7 °C in winter [27]. The lake is characterized by the presence of thermal water vents, previously describe by [28], which show same differences from lake water: (i) ionic strength ranges from 0.024 to 0.222 M in thermal water, and between 0.004 and 0.443 M in lake water; (ii) pH variates between 5.8 and 7.1, and Eh between 0.01 and 0.17 V, in thermal water, while lake water exhibits pH between 8 and 10, and Eh from −0.29 and 0.01 V; (iii) lake water preferentially falls in the field of alkaline elements, while thermal water fell between alkaline and Ca^{2+}-rich field (see [29] for details).

Presently, Lake Van is a monomictic system, undergoing at least partial mixing [30], and it is anoxic below a depth of 300 m [20,24]. Thermal stratification in the summer is induced by the warming of the upper 10 to 15 m surface layer to temperatures between 17 and 20 °C [20]. Water temperature then falls to a minimum of 3 °C between 40 m and 50 m depth. Concurrently, a minor increase in salinity is observed, rising from 21.9 psu at the surface to 22.5 psu at 100 m depth [20]. The inflow of freshwater during spring and early summer slightly reduces both the total salinity and alkalinity of the surface layer. Biological activity in spring and summer typically leads to an increase in surface pH (resulting from CO_2 consumption) and a decrease in the pH of the hypolimnion (due to the degradation of organic matter). The photic zone extends to 35 m deep for most of the year, deepening to 50 m during the winter months [31].

The Van area receives approximately 400 mm/yr of direct annual precipitation, primarily as winter snow and spring rain [32], whereas the maximum input of runoff occurs in late spring and early summer, driven by snowmelt from the surrounding mountains.

Inter-annual fluctuations in lake level have been significant, ranging from a minimum of 1646.69 m asl in January 1963 to a maximum of 1650.55 m asl in June 1995, with a typical seasonal change of 0.42 m [33,34].

Hydrochemistry of Lake Van, its contributing rivers, and sub-lacustrine springs has been analyzed by [20,21]. Rivers draining carbonate terrains supply bicarbonate and Ca-rich waters, while those draining Quaternary volcanic rocks deliver bicarbonate, alkaline elements (Na and K), chloride, and sulfate. River waters generally have a molar Mg/Ca of 2:1 and are undersaturated with respect to calcite and aragonite [20].

Sub-lacustrine spring waters in the southwest show an average molar Mg/Ca of 0.79, average pH of 7.5, and average alkalinity of 16.16 meq L^{-1}, and are undersaturated to slightly oversaturated with respect to carbonates, with higher alkaline element contents than river waters [29].

Whiting (milky carbonate precipitation, mainly calcite) occurs at river mouths, caused by the mixing of Ca-rich river water with the highly carbonate-rich lake water. The lake sediments are varved due to a lack of benthic activity (e.g., [35,36]. Varve analysis reveals seasonal carbonate precipitation: Ca-rich light laminae are made of aragonite, forming during late summer with low runoff and high evaporation, while Si–Mg-rich dark laminae are made of calcite, precipitating during high spring runoff, with associated siliciclastic input.

3. Sampling and Analytical Methods

Sampling operations in Lake Van were carried out on 26–28 October 2023. Samples were taken from 11 different points along the shore, as shown in Figure 1 and Table 1. At the time of stromatolite sampling, a water sample was also taken at 20 cm below the lake surface, in the immediate vicinity of the solid samples.

Table 1. Sampling sites and geographic coordinates of the lake Van water.

Sample	Location	Longitude (E)	Latitude (N)
ST1	Tatvan	42.305124°	38.482524°
ST2	Adabağ	42.452715°	38.637806°
ST3	Ahlat	42.532471°	38.759970°
ST4	Adilcevaz	42.795610°	38.786339°
ST5	Ercis W	43.279248°	38.959671°
ST6	Ercis E	43.530767°	38.984128°
ST7	Edremit E	43.311378°	38.431562°
ST8	Edremit SW	43.180271°	38.382668°
ST9	Hasbey	42.941726°	38.329994°
ST10	Bolalan	42.687062°	38.429276°
ST11	Tatvan E	42.436072°	38.505397°

Stromatolite samples were crushed, powdered to approximately 200 mesh size, and sent to the Acme-Canada laboratory (Vancouver, Canada) for analysis. Here, the main oxide analyses were performed using ICP-AES, while trace element and REE analyses were performed using ICP-MS. Sample preparation involved digesting 50 mg of powdered stromatolite samples in an HCl:HNO_3:H_2O solution (1:1:1, *v*/*v*; 6 mL per 1.0 g sample) for one hour. Digested samples were then analyzed for main oxide, trace, and REE. The accuracy of determinations was checked with certified reference materials (Supplementary Materials). The accuracy of measurement was better than 0.01% for SiO_2, Al_2O_3, Fe_2O_3, MgO, CaO, NaO, K_2O, better than 0.05% for MnO, and 0.001% for TiO_2. The accuracy of REE analyses was better than 0.01 ppm for Pr, Sm, Gd, Tb, Dy, Ho, Er, better than 0.05 for La, Ce, Nd, better than 0.002 ppm for Lu, and 0.005 ppm for Eu and Tm.

XRD analyses were performed only on samples ST3 and ST7, representative of the extremes of the mineralogical spectrum of Lake Van stromatolites. Bulk mineralogy was determined by powder X-ray diffraction (XRD, at Yebim Laboratory, Ankara University, Turkey) using Cu-Kα radiation filtered by a monochromatic crystal and a scanning speed of 2° 2θ/min. The relative proportions of minerals were established according to the methods and data of [37].

4. Results

4.1. Mineralogy and Major Element Geochemistry

XRD analysis results and XRD spectra are given in Table 2 and Figure 2.

Table 2. Mineralogical phases of stromatolites (%).

Sample	Calcite	Quartz	Dolomite	Feldspar	Clay m
ST3	85.45	10.92	2.41		1.22
ST7	72.15	18.92	5.24	2.48	1.22

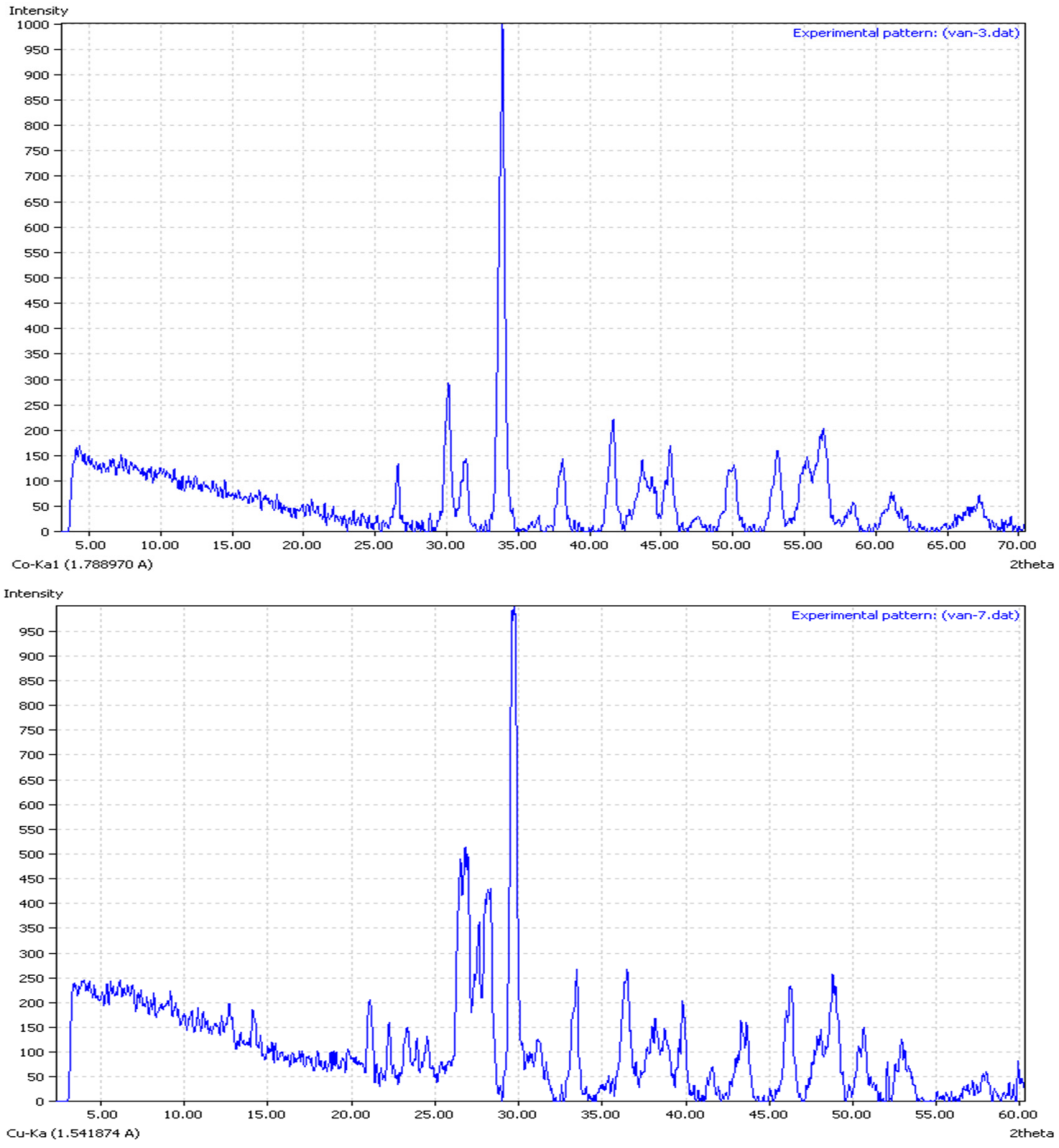


Figure 2. X-ray diffraction pattern for ST3 and ST7 stromatolite samples in Lake Van.

Sample ST3 represents the carbonate-dominant group, defined by high chemical purity and a predominance of authigenic minerals. In contrast, Sample ST7 represents the detrital-influenced group, characterized by a significant influx of terrigenous components. By focusing on these two representative samples, we can effectively capture the fundamental variability between the lake's internal precipitation processes and external river-driven inputs. A brief description of the mineralogical results for the two analyzed samples: (i) sample ST3 is predominantly composed of Calcite (85.45%), followed by Quartz (10.92%). It contains minor proportions of Dolomite (2.41%) and Clay minerals (1.22%), while Feldspar is absent; (ii) sample ST7 consists of 72.15% Calcite and 18.92% Quartz. It also contains 5.24% Dolomite, 2.48% Feldspar, and 1.22% Clay minerals.

Looking at the major oxide composition (see Supplementary Materials Table S1), stromatolites can be divided into two main groups: the first group is enriched in SiO_2, and the second one in CaO. Stromatolites have a variable amount of SiO_2, ranging from 0.70 to 57.3%, while CaO spans between 9.31 and 53.3%. Samples with the higher silica amount show the higher Al_2O_3, TiO_2, Fe_2O_3, Na_2O, K_2O, and TiO_2 contents (Figure 3).

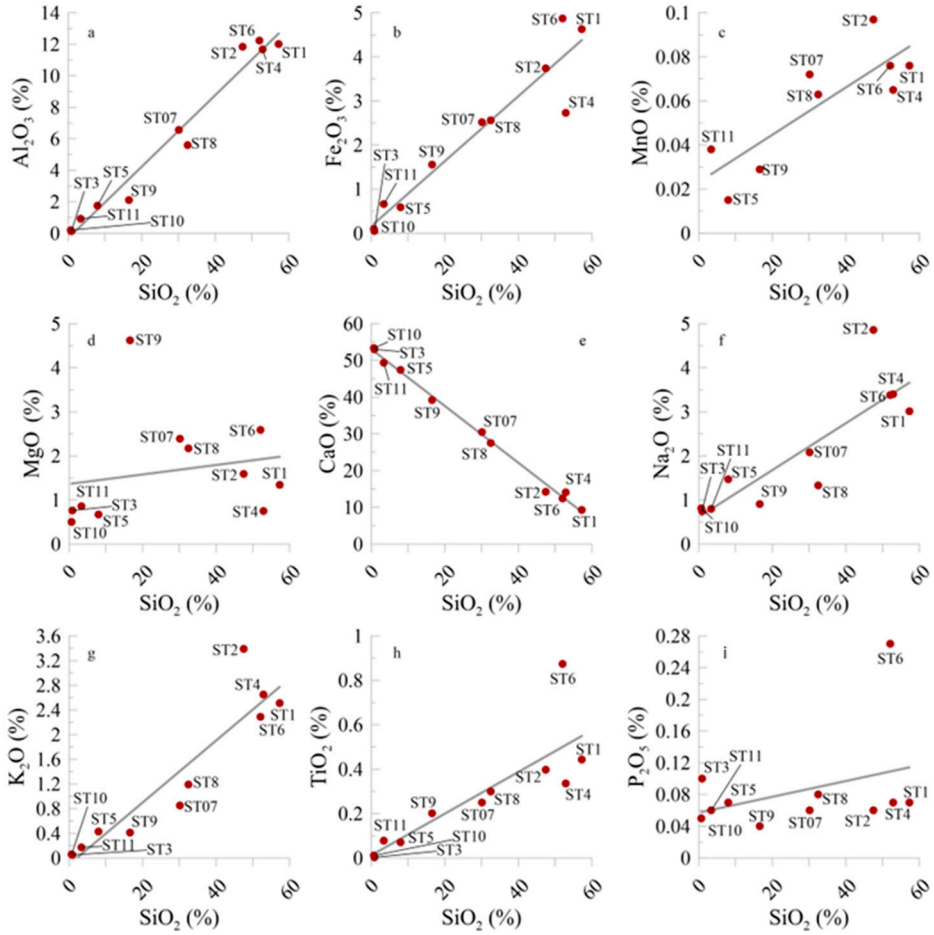


Figure 3. Binary diagrams of major oxides in stromatolite samples from Lake Van: (**a**) SiO_2 vs. Al_2O_3; (**b**) SiO_2 vs. Fe_2O_3; (**c**) SiO_2 vs. MnO; (**d**) SiO_2 vs. MgO; (**e**) SiO_2 vs. CaO; (**f**) SiO_2 vs. Na_2O; (**g**) SiO_2 vs. K_2O; (**h**) SiO_2 vs. TiO_2; (**i**) SiO_2 vs. P_2O_5.x.

By summarizing bulk-sediment major element compositions on ternary plots (Figure 4a), the data distribution indicates that the main difference in stromatolites' geochemistry is expressed by variable MgO + CaO contents, with samples ST3, ST10, and ST11 the most enriched in the carbonate fraction. The strong positive correlation observed in binary diagrams (Figure 3) between SiO_2 and oxides such as Al_2O_3, Fe_2O_3, and K_2O clearly defines a detrital trend. Conversely, the negative correlation between SiO_2 and CaO (Figure 3e)

illustrates a dilution effect, where the increase in terrigenous input progressively masks the authigenic carbonate precipitation. This is particularly evident when comparing the carbonate-dominant samples (ST3, ST10, and ST11).

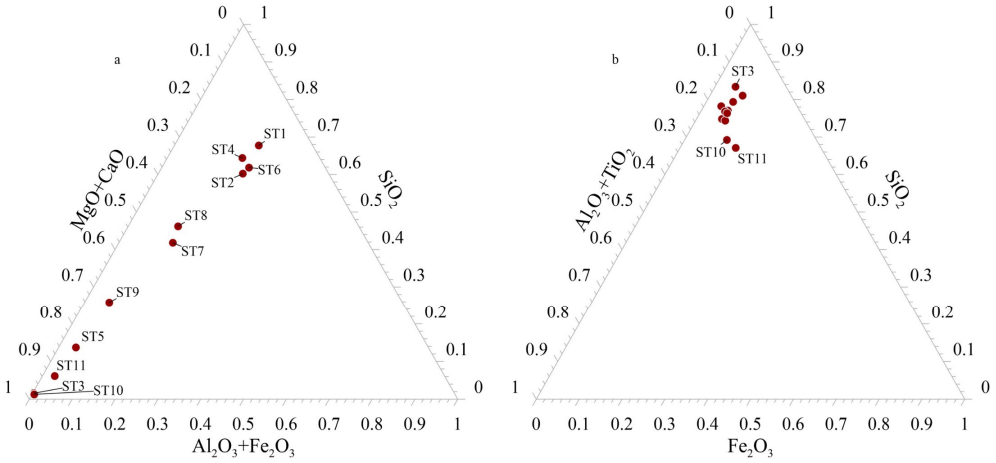


Figure 4. Ternary diagram: (**a**) $Al_2O_3 + Fe_2O_3 - SiO_2 - MgO + CaO$; (**b**) $Fe_2O_3 - SiO_2 - Al_2O_3 + TiO_2$ in stromatolite samples from lake Van.

Following [38], the amount of $CaCO_3$ (%) has been calculated from the total Ca concentration (Ca_{tot}), with a correction for the Ca inventory supported by the detrital component:

$$CaCO_3 = 2.5\,[Ca_{tot} - (Al_{tot} \times Ca/Al_{average\ shale})]$$

where the $Ca/Al_{average\ shale}$ value is 0.276. Calculated $CaCO_3$ values range from 12.2 to 95.2%. The most $CaCO_3$-enriched samples are ST10, ST3, and ST11.

The contribution of the detrital component is shown in the ternary plots (Figure 4a,b). As shown in the ternary diagram (Figure 4a), samples ST3, ST10, and ST11 are positioned near the MgO + CaO vertex, representing the end-members of the authigenic fraction. This distribution confirms that their formation process is mainly controlled by the alkaline hydrochemical context of the basin, with a negligible influence of the terrigenous siliciclastic component. In contrast, the data cluster near the top of the diagram (Figure 4a), close to the SiO_2 vertex, indicates detrital components enriched in silicates.

4.2. Minor Element Abundances

Minor element concentrations are listed in Supplementary Materials Table S2. The total amount of minor elements ranges between 0.3 (for Cs) and 5799 ppm (Sr). Samples ST3, ST7, ST10, and ST11 are particularly enriched in Sr and show very low concentrations in Zr (namely of detrital origin). Strontium and calcium have similar ionic charges and relatively similar ionic radii and can substitute for each other in carbonates. This similarity allows Sr^{2+} to be incorporated into the carbonate lattice by replacing Ca^{2+}, particularly in the aragonite structure.

Elements with a possible vital effect, such as V, Cr, Co, Ni, Cu, Zn, Mo, Sn, and Sb, have noteworthy concentrations in many carbonates [39], even if they are also of silicoclastic origin. Minor element abundances showing concentration higher than in the continental crust [40] confirm a clear geochemical separation between the sampled sites. In particular, samples ST3, ST10, and ST11 record the lowest concentrations of lithogenic elements. Sample ST3 shows the lowest values overall, with concentrations of Sc, V, Co, Rb, Nb, and Cs below the limits of detection (LOD). Similarly, the sample ST10 shows values below LOD for Sc, V, Co, Nb, and Cs, with an extremely low concentration of Rb (1 ppm). Furthermore, the sample ST11 shows Sc and Co below the limits of detection, and sample ST5 shows

only Co below this threshold. Despite the moderate silicoclastic content of these samples, no particular correlation can be confirmed between Si and these elements.

4.3. Rare Earth Elements

The REE contents are listed in Supplementary Materials Table S3. Total REE abundance (ΣREE) exhibits significant variability across the sampling sites, ranging from a minimum of 0.25 ppm in sample ST3 to a maximum of 12 ppm in sample ST2. Low amounts of REE are also shown by ST10 (0.25 ppm) and ST11 (0.93 ppm). In addition to the ST2 sample, the highest ΣREE concentration is shown by samples ST1 (11.45 ppm) and ST4 (10.44 ppm).

The ΣREE concentration is positively correlated to Si (%), Al (%), and Fe (%), and negatively correlated to CaO_3(%) (Figure 5).

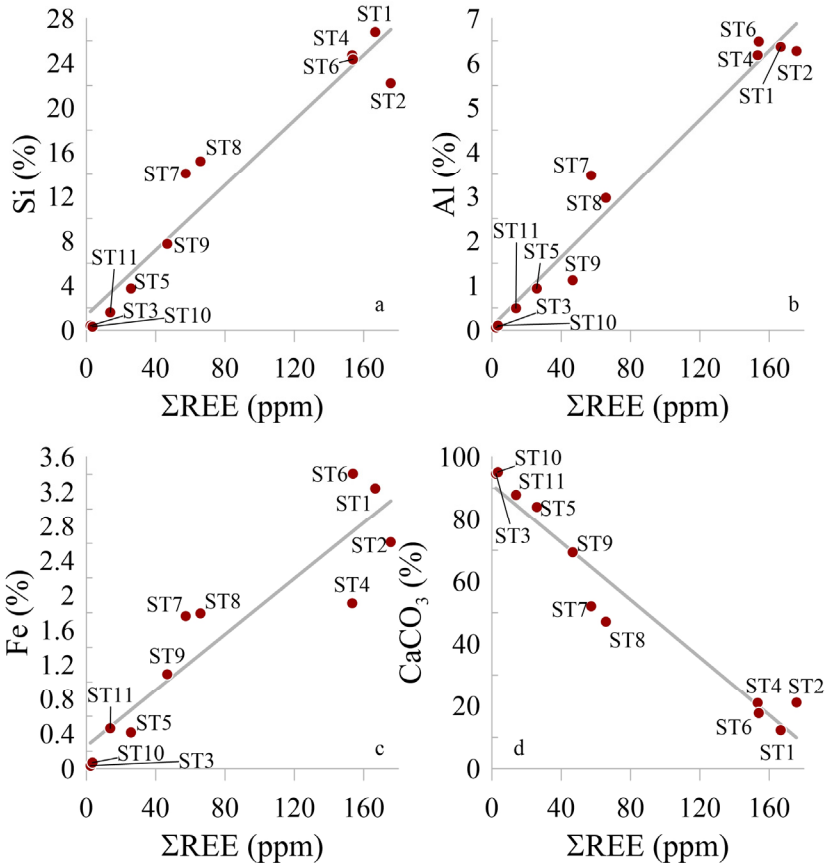


Figure 5. Binary diagrams ΣREE (ppm) vs. (**a**) Si (%), (**b**) Al (%), (**c**) Fe (%), and (**d**) $CaCO_3$ (%) in stromatolite samples from Lake Van.

The strong negative correlation observed between ΣREE and $CaCO_3$(%) confirms that REE are not hosted within the carbonate lattice, but they are instead carried by the detrital fraction (Si-Al-Fe-rich minerals). Consequently, samples with the highest carbonate purity, such as ST3, ST10, and ST11, exhibit the lowest ΣREE concentrations.

The shale-normalized (to Post-Archean Australian Shale; ppm and PAAS; [41]), REE patterns of stromatolites (Figure 6) highlight different distributions between samples. In general, it is possible to distinguish two main sample groups, which move from a flat trend to a progressive enrichment in HREE (ST3, ST10, ST11, and to a lesser extent in ST5). Samples showing the lowest concentrations are the same with a progressive enrichment in HREE and high $CaCO_3$ contents (ST3, ST10, and ST11), reflecting the specific hydrochemistry of Lake Van. In high-alkalinity waters, HREEs preferentially form stable dicarbonate complexes, such as $[REE(CO_3)_2]^-$ [42,43]. These complexes increase the

solubility of HREEs relative to Light REEs (LREEs), resulting in the characteristic HREE-enriched patterns recorded during authigenic carbonate precipitation. This signature is further corroborated by the La/Yb ratio, lower in ST3, ST10, and ST11. These findings confirm that these stromatolites act as reliable archives of the lake's aqueous geochemistry. Furthermore, REEs show a good correlation with lithogenic proxies like Si, Al, and Fe; consequently, the samples with the most remarkable HREE enrichment are those with the lowest concentrations of these detrital elements.

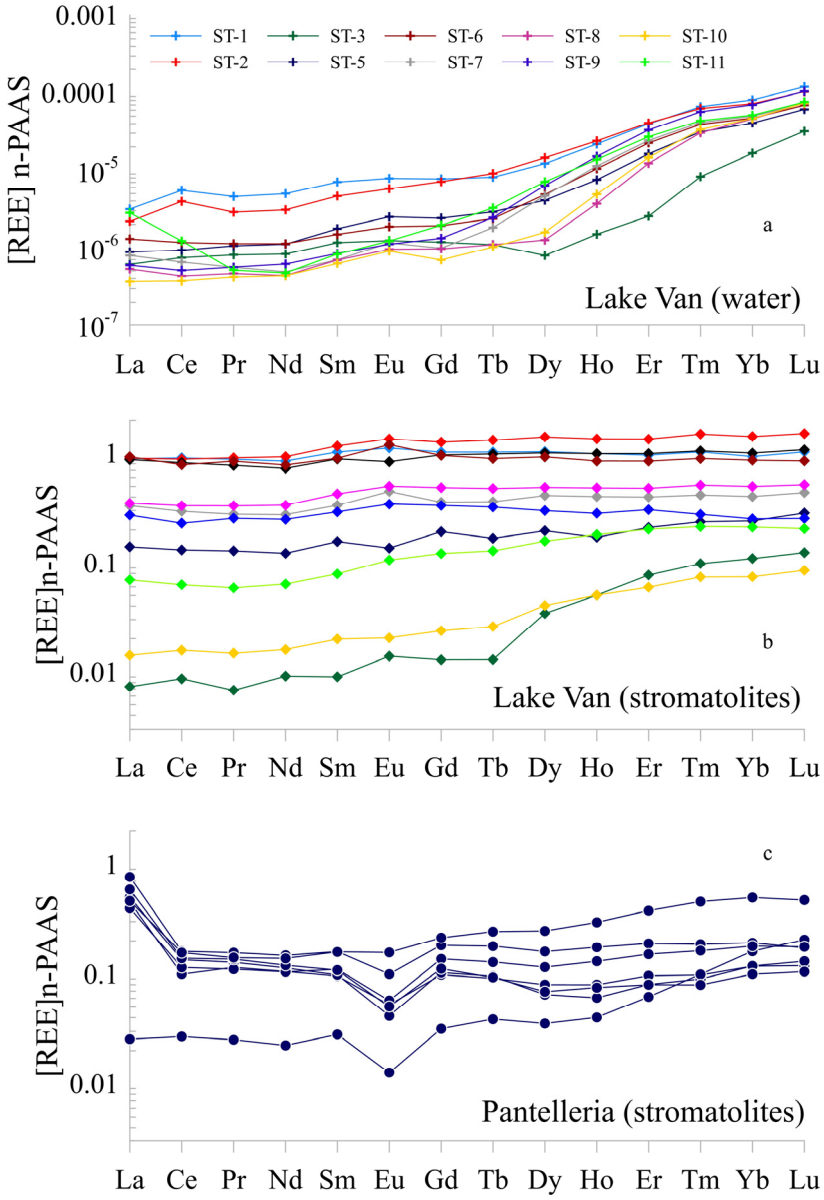


Figure 6. (**a**) REE distribution patterns of Lake Van water; (**b**) Lake Van stromatolites (symbol colors used for stromatolites are the same as water in the same site); (**c**) Lake Specchio di Venere stromatolites (Pantelleria, Italy).

Y and Ho, as well as Zr and Hf pairs, are well correlated (Figure 7). Y/Ho ratio shows values from slightly subchondritic to superchondritic, with the highest values in the sample enriched in $CaCO_3$. Zr/Hf ratios are always superchondritic, with the exception of samples ST3 (chondritic) and ST10 (subchondritic).

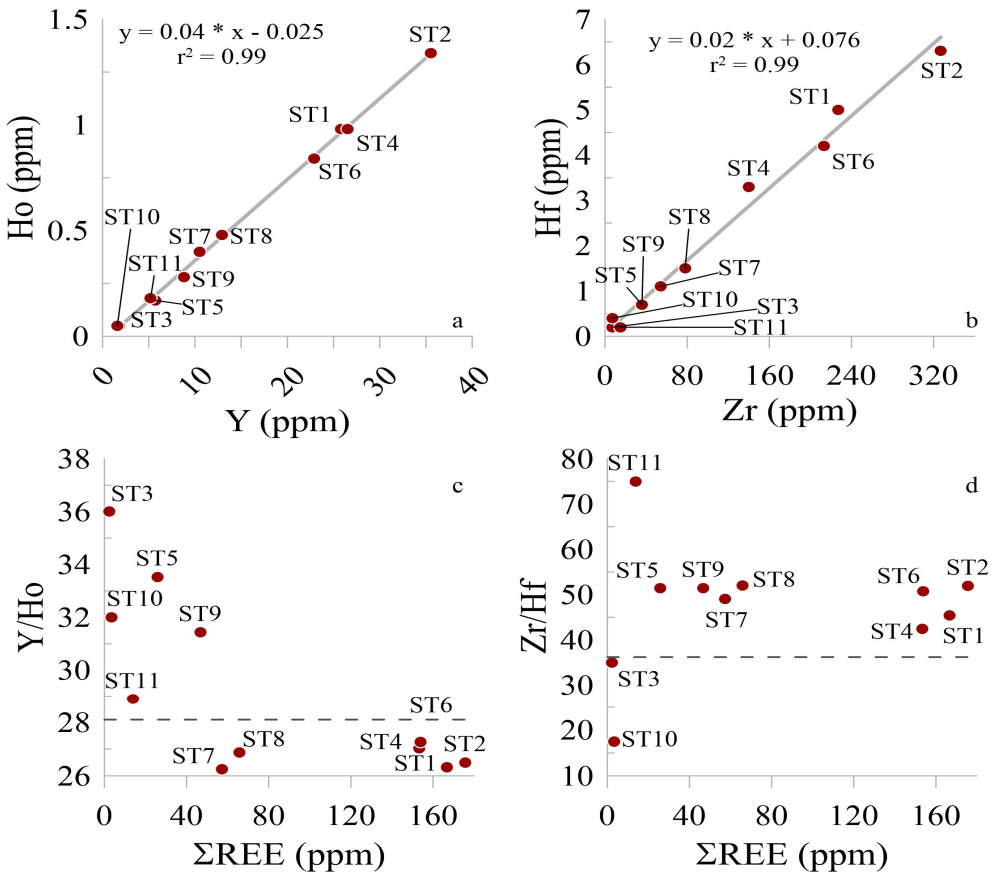


Figure 7. (**a**) Y vs. Ho; (**b**) Zr vs. Hf; (**c**) ΣREE vs. Y/Ho; (**d**) ΣREE vs. Zr/Hf in stromatolite samples from Lake Van.

5. Discussion

The mineralogical composition of samples ST3 and ST7 reflects the competitive interplay between autochthonous lacustrine precipitation and allochthonous detrital influx. Sample ST3 represents the carbonate-dominant facies, characterized by a high Calcite content (85.45%) and a relatively low siliciclastic fraction (10.92% Quartz and 1.22% Clay minerals). This composition suggests a depositional environment dominated by endogenic chemical precipitation, driven by the lake's high alkalinity, where the carbonate precipitation prevailing in the water column is relatively undisturbed by detrital inputs. In contrast, ST7 serves as the more detrital-richer endmember, showing a significant dilution of the carbonate matrix (72.15% Calcite) by an increased terrigenous load. The rise in Quartz (18.92%) and the diagnostic presence of Feldspar (2.48%) in ST7 indicate a closer proximity to fluvial discharge points, or periods of intensified river runoff, where weathering products from the surrounding volcanic and metamorphic catchments are actively transported into the basin.

This mineralogical variability is intrinsically linked to the high-resolution seasonal depositional cycles and microbial processes, documented in the region. According to the recent study by [36], the sedimentary record of Lake Van is defined by annually laminated (varved) sequences. These consist of light-colored laminae, primarily composed of authigenic calcium carbonate (calcite) precipitated during the spring and summer (matching the profile of ST3), and dark-colored laminae, which represent the delivery of siliciclastic detritus (quartz, feldspar, and clay) during high-energy seasonal river discharge or runoff events (aligned with ST7).

Furthermore, Çağatay et al. [35] highlight that these mineralogical signatures are influenced by the same alkaline conditions that facilitate the growth of the lake's massive stromatolites on the northern shelf. The balance between the carbonate precipitation seen in ST3 and the detrital masking in ST7 serves as a sensitive proxy for understanding the shifting hydroclimatic conditions, the evolution of the lake's unique alkaline ecosystem, and the specific geochemical environment required for stromatolites' morphogenesis.

The good positive correlation between ∑REE and lithogenic proxies such as Si, Al, and Fe indicates that the total REE budget is overwhelmingly dominated by the detrital fraction. This is consistent with the findings of [44], who demonstrated that even minor amounts of siliciclastic contamination can mask the primary REE signal, due to the several orders of magnitude higher REE concentrations in shales compared to carbonates.

Samples with high $CaCO_3$ (ST3, ST10, ST11) represent the most pristine end-members of stromatolite formation. The authigenic origin of the purest carbonate fractions (ST3, ST10, ST11) is further confirmed by the comparison with the chemistry of the lake waters described by [10]. In these samples, the low ∑REE values (approaching the ppb range) allow the primary lake water signature to emerge. The observed enrichment in HREE relative to LREE is a hallmark of alkaline, carbonate-rich waters, where HREEs form more stable dissolved carbonate complexes (e.g., $[Ln(CO_3)_2]^-$), as discussed by [41].

Furthermore, according to [10], REE patterns of lake water show trends similar to those recorded in the most pristine authigenic carbonate samples, in particular ST3, ST10, and ST11. This coincidence demonstrates that no significant fractionation of REE occurs during the inorganic precipitation of carbonate minerals (calcite and aragonite). Consequently, samples ST3, ST10, and ST11 represent the hydrochemical composition of the water column at the time of their formation, facilitated by the extreme alkaline conditions of the lake.

The Y/Ho ratios in stromatolites provide further evidence of their authigenic origin. While detrital materials typically exhibit chondritic Y/Ho ratios (~26–28), the most carbonate-pure samples show superchondritic values. In primary geological processes, such as the formation of magma and the subsequent crystallization of igneous minerals, Y and Ho are often described as "geochemical twins", because their behavior is strictly governed by their nearly identical ionic radii and charges, termed CHARAC (CHarge And RAdius Controlled) by [45]; these elements do not fractionate significantly in magmatic rocks, typically maintaining the standard chondritic ratio of approximately 28. Samples showing chondritic Y/Ho ratio are the same characterized by a flat HREE pattern, suggesting that these stromatolites inherited their geochemical signature from a significant detrital input rather than from authigenic precipitation. However, as highlighted by [46], this symmetry breaks down when these elements enter the world of aqueous reactions and carbonate precipitation. In these environments, we move into non-CHARAC processes, where the physical size of the ions becomes less important than their outer electronic configuration. While Yttrium has a [Kr]4d0 structure, Holmium possesses a [Xe]4f10 configuration. This subtle difference in their "electronic shells" means they react differently to ligands and mineral surfaces; Holmium is more easily removed from water through scavenging, while Yttrium tends to stay in solution. Consequently, when carbonates precipitate from a water phase enriched in Y, they capture a "supercondritic" signature, reflecting a complex history of chemical interactions rather than a simple magmatic process.

Furthermore, the Zr/Hf ratios, which remain largely superchondritic, with the exception of the most carbonate-enriched samples (ST3 and ST10), suggest a transition from a detritus-dominated system to another one controlled by chemical precipitation. The subchondritic Zr/Hf in ST10 might reflect specific local conditions or could be related to the "vital effect" described by [47], where microbial biofilms actively influence the

uptake of transition and trace elements, although this hypothesis should be confirmed by further investigations.

The REE distribution patterns of stromatolites from Lake Van (Figure 6) show remarkable similarities to those of the Specchio di Venere Lake (Pantelleria). Both systems are characterized by alkaline, high-pH waters, which promote the formation of HREE-enriched carbonate precipitates. Cangemi et al. [10] demonstrated that the stability constants of REE complexes, in the lake water, from which carbonates precipitate, follow the diminishing sequence $[REE(CO_3)_2]^-$ >> $[REE(CO_3)]^+$, as formerly found by Sasmaz et al. [28]. However, Lake Van stromatolites exhibit a more pronounced influence of detrital inputs, likely due to the wider extension of its catchment areas. This comparison underscores the sensitivity of microbialite geochemistry to both global chemical principles (carbonate complexation) and local sedimentological settings.

6. Conclusions

Mineralogical data and REE distribution patterns reveal a clear division of Lake Van stromatolites into two primary geochemical groups. The first group, comprising sites ST3, ST10, and ST11, represents the authigenic end-members of the system, characterized by high chemical purity ($CaCO_3$ > 85%) and minor siliciclastic content. In contrast, the other samples are dominated by a detrital overprint, rich in silica and volcanic-derived minerals. Ternary diagrams support this classification, showing a distinct alignment of the data toward a purely carbonate end-member. Furthermore, the robust correlation between ∑REE_ and Al-Si-Fe confirms that, even in high-alkalinity environments, the total REE budget is overwhelmingly controlled by the detrital fraction. These findings emphasize that a multi-proxy approach is essential to carefully filter out lithogenic influences and isolate the primary geochemical signatures inherited from the lake water, pointing to the conclusion that Lake Van represents a complex geochemical system, regulated by a dynamic balance between hydrothermal inputs and the surface hydrological dynamics. The input of CO_2, primarily linked to the activity of the Mount Nemrut volcanic system, combined with evaporative phenomena, and the influx of runoff and groundwater, creates an extremely alkaline environment, rich in carbonate species. In this context, the formation of massive stromatolites is the result of constant competition between authigenic carbonate precipitation and the influx of volcanic siliciclastic detritus, transported from the surrounding drainage basins.

The approach we followed in the description of this highly complex lacustrine system could be successfully applied in similar environments, differently located worldwide, but taking into account the limitations of the REE-Y/Ho-Zr/Hf proxy system.

These two twins significantly fractionate during water-rock interaction processes, which lead to the formation of authigenic minerals, whose surface properties are suspected to be a driver of Y-Ho and Zr-Hf fractionations. The quantitative description of these processes is presently poorly known, and further investigations are required to clarify their role.

Supplementary Materials: The following supporting information can be downloaded at: https://www.mdpi.com/article/10.3390/min16020224/s1. Table S1: major oxides (%); Table S2: trace elements (ppm); Table S3: rare earth elements (ppm).

Author Contributions: Conceptualization, B.S., M.C. and A.S.; methodology, A.S.; software, M.C. and Y.O.; validation, B.S., M.C. and A.S.; formal analysis, M.C.; investigation, B.S. and A.S.; resources, M.C. and Y.O.; data curation, M.C. and Y.O.; writing—original draft preparation, M.C. and Y.O.; writing—review and editing, M.C., Y.O. and A.S.; visualization, A.S.; supervision, M.C., B.S. and

A.S.; project administration, A.S.; funding acquisition, A.S. All authors have read and agreed to the published version of the manuscript.

Funding: This research was funded by Firat University with MF.25.97 projects (A.S.).

Data Availability Statement: The original contributions presented in this study are included in the article. Further inquiries can be directed to the corresponding author.

Acknowledgments: This research was funded by Firat University with MF.25.97 projects. We wish to thank the two anonymous reviewers for their precious suggestions.

Conflicts of Interest: The authors declare no conflicts of interest.

References

1. Burne, R.V.; Moore, L.S. Microbialites: Organosedimentary deposits of benthic microbial communities. *Palaios* **1987**, *2*, 241–254. [CrossRef]
2. Awramik, S.M. The history and significance of stromatolites. In *Early Organic Evolution: Implications for Energy and Mineral Resources*; Schidlowski, M., Kimberley, M.M., McKirdy, D.M., Trudinger, P.A., Eds.; Springer: Berlin, Germany, 1992; pp. 435–449. [CrossRef]
3. Cangemi, M.; Bellanca, A.; Borin, S.; Hopkinson, L.; Mapelli, F.; Neri, R. The genesis of actively growing siliceous stromatolites: Evidence from Lake Specchio di Venere, Pantelleria Island, Italy. *Chem. Geol.* **2010**, *276*, 318–330. [CrossRef]
4. Censi, P.; Cangemi, M.; Madonia, P.; Saiano, F.; Brusca, L.; Zuddas, P. Discrimination between effects induced by microbial activity and water-rock interactions under hydrothermal conditions according to REE behavior. *Procedia Earth Planet. Sci.* **2013**, *7*, 123–126. [CrossRef]
5. Censi, P.; Cangemi, M.; Brusca, L.; Madonia, P.; Saiano, F.; Zuddas, P. The behavior of rare-earth elements, Zr and Hf during biologically-mediated deposition of silica-stromatolites and carbonate-rich microbial mats. *Gondwana Res.* **2015**, *27*, 209–215. [CrossRef]
6. Cangemi, M.; Censi, P.; Reimer, A. Carbonate precipitation in the alkaline lake Specchio di Venere (Pantelleria Island, Italy) and the possible role of microbial mats. *Appl. Geochem.* **2016**, *67*, 168–176. [CrossRef]
7. Cangemi, M.; Madonia, P.; Bellomo, S.; Oliveri, Y. Geochemical and isotopic characterisation of actual lacustrine sediments from the hydrothermal lake Specchio di Venere, Pantelleria Island (Italy). *J. Chem.* **2016**, *2016*, 8414581. [CrossRef]
8. Cangemi, M.; Madonia, P.; Speziale, S. Geochemistry and mineralogy of a complex sedimentary deposit in the alkaline volcanic Lake Specchio di Venere (Pantelleria Island, south Mediterranean). *J. Limnol.* **2018**, *77*, 220–231. [CrossRef]
9. Kaya, M.; Yildirim, B.A.; Kumral, M.; Sasmaz, A. Trace and rare earth element (REE) geochemistry of recently formed stromatolites at Lake Salda, SW Turkey. *Water* **2023**, *15*, 733. [CrossRef]
10. Cangemi, M.; Oliveri, Y.; Sasmaz, B.; Censi, P.; Sasmaz, A. Potential function of microbial mats in regard to water chemistry and carbonate precipitation in the alkaline waterbody Lake Van (Turkey). *Water* **2025**, *17*, 2060. [CrossRef]
11. Visscher, P.T.; Stolz, J.F. Microbial mats as bioreactors: Populations, processes, and products. In *Stromatolites: Geobiology, Paleontology, and Photoenergy Settings*; Vinogradov, S.N., Seckbach, J., Eds.; Springer: Dordrecht, The Netherlands, 2005; pp. 163–200. [CrossRef]
12. Dupraz, C.; Reid, R.P.; Braissant, O.; Decho, A.W.; Norman, R.S.; Visscher, P.T. Processes of carbonate precipitation in modern microbial mats. *Earth-Sci. Rev.* **2009**, *96*, 141–162. [CrossRef]
13. Glunk, C.; Dupraz, C.; Braissant, O.; Gallagher, K.L.; Verrecchia, E.P.; Visscher, P.T. Microbially mediated carbonate precipitation in a hypersaline lake, Big Pond (Eleuthera, Bahamas). *Sedimentology* **2009**, *58*, 720–736. [CrossRef]
14. Arp, G.; Reimer, A.; Reitner, J. Photosynthesis-induced biofilm calcification and calcium concentrations in Phanerozoic oceans. *Science* **2001**, *292*, 1701–1704. [CrossRef]
15. Gallagher, K.L.; Kading, T.J.; Braissant, O.; Dupraz, C.; Visscher, P.T. Inside the alkalinity engine: The role of electron donors in the organomineralization potential of sulfate-reducing bacteria. *Geobiology* **2012**, *10*, 518–530. [CrossRef]
16. Peters, S.E.; Husson, J.M.; Wilcots, J. The rise and fall of stromatolites in shallow marine environments. *Geology* **2017**, *45*, 487–490. [CrossRef]
17. Riding, R. Microbial carbonates: The geological record of calcified bacterial–algal mats and biofilms. *Sedimentology* **2000**, *47*, 179–214. [CrossRef]
18. Garrett, P. Phanerozoic stromatolites: Noncompetitive ecologic restriction by grazing and burrowing animals. *Science* **1970**, *169*, 171–173. [CrossRef]

19. Reid, R.P.; Visscher, P.T.; Decho, A.W.; Stolz, J.F.; Bebout, B.M.; Dupraz, C.; Macintyre, I.G.; Paerl, H.W.; Pinckney, J.L.; Prufert-Bebout, L.; et al. The role of microbes in accretion, lamination and early lithification of modern marine stromatolites. *Nature* **2000**, *406*, 989–992. [CrossRef] [PubMed]
20. Reimer, A.; Landmann, G.; Kempe, S. Lake Van, Eastern Anatolia, hydrochemistry and history. *Aquat. Geochem.* **2009**, *15*, 195–222. [CrossRef]
21. Kempe, S.; Kazmierczak, J.; Landmann, G.; Konuk, T.; Reimer, A.; Lipp, A. Largest known microbialites discovered in Lake Van, Turkey. *Nature* **1991**, *349*, 605–608. [CrossRef]
22. Lopez-Garcia, P.; Kazmierczak, J.; Benzerara, K.; Kempe, S.; Guyot, F.; Moreira, D. Bacterial diversity and carbonate precipitation in the giant microbialites from the highly alkaline Lake Van, Turkey. *Extremophiles* **2005**, *9*, 263–274. [CrossRef]
23. Benzerara, K.; Menguy, N.; López-García, P.; Yoon, T.H.; Kazmierczak, J.; Tyliszczak, T.; Guyot, F.; Brown, G.E., Jr. Nanoscale detection of organic signatures in carbonate microbialites. *Proc. Natl. Acad. Sci. USA* **2006**, *103*, 9440–9445. [CrossRef]
24. Stockhecke, M.; Sturm, M.; Brunner, I.; Schmincke, H.U.; Sumita, M.; Kipfer, R.; Cukur, D.; Kwiecien, O.; Anselmetti, F.S. Sedimentary evolution and environmental history of Lake Van (Turkey) over the past 600,000 years. *Sedimentology* **2014**, *61*, 1830–1861. [CrossRef]
25. Ates, Y.; Yakupoglu, T. Assessment of lacustrine/fluvial clays as liners for waste disposal (Lake Van Basin, Turkey). *Environ. Earth Sci.* **2012**, *67*, 653–663. [CrossRef]
26. Möller, P.; Bau, M. Rare-earth patterns with positive cerium anomaly in alkaline waters from Lake Van, Turkey. *Earth Planet. Sci. Lett.* **1993**, *117*, 671–686. [CrossRef]
27. Kavak, M.T.; Karadoğan, S. The relationship between sea surface temperature and chlorophyll concentration of phytoplanktons in the Black Sea using remote sensing techniques. *J. Environ. Biol.* **2012**, *33*, 493–498.
28. Sasmaz, A.; Zuddas, P.; Cangemi, M.; Piazzese, D.; Ozek, G.; Venturi, M.; Censi, P. Zirconium and hafnium fractionation and distribution of rare earth elements in neutral–alkaline waters: Case study of Lake Van hydrothermal system, Turkey. *J. Geochem. Explor.* **2021**, *226*, 106784. [CrossRef]
29. Kremer, B.; Kaźmierczak, J.; Kempe, S. Authigenic replacement of cyanobacterially precipitated calcium carbonate by aluminium-silicates in giant microbialites of Lake Van (Turkey). *Sedimentology* **2018**, *66*, 285–304. [CrossRef]
30. Kipfer, R.; Aeschbach-Hertig, W.; Baur, H.; Hofer, M.; Imboden, D.M.; Signer, P. Injection of mantle type helium into Lake Van (Turkey): The clue for quantifying deep water renewal. *Earth Planet. Sci. Lett.* **1994**, *127*, 15–26. [CrossRef]
31. Huguet, C.; Fietz, S.; Stockhecke, M.; Sturm, M.; Anselmetti, F.S.; Rosell-Melé, A. Biomarker seasonality study in Lake Van, Turkey. *Org. Geochem.* **2011**, *42*, 1289–1298. [CrossRef]
32. Kadioğlu, M.; Şen, Z.; Batur, E. The greatest soda-water lake in the world and how it is influenced by climatic change. *Ann. Geophys.* **1997**, *15*, 1489–1497. [CrossRef]
33. E.I.E.I. *Lake Levels*; Elektrik Idaresi Etut Isleri Genel Mudurlugu Yayını: Ankara, Turkey, 1996.
34. E.I.E.I. *Lake Levels*; Elektrik Idaresi Etut Isleri Genel Mudurlugu Yayını: Ankara, Turkey, 2008.
35. Çağatay, M.N.; Öğretmen, N.; Damcı, E.; Stockhecke, M.; Sancar, Ü.; Eriş, K.K.; Özeren, S. Lake level and climate records of the last 90 ka from the northern basin of Lake Van, eastern Turkey. *Quat. Sci. Rev.* **2014**, *104*, 97–116. [CrossRef]
36. Çağatay, M.N.; Damcı, E.; Bayon, G.; Sarı, M. Microbialites on the northern shelf of Lake Van, eastern Türkiye: Morphology, texture, stable isotope geochemistry and age. *Sedimentology* **2023**, *71*, 433–463. [CrossRef]
37. Schultz, L.G. *Quantitative Interpretation of Mineralogical Composition from X-Ray and Chemical Data for the Pierre Shale*; U.S. Geological Survey Professional Paper 391-C; U.S. Government Printing Office: Washington, DC, USA, 1964.
38. Turekian, K.K.; Wedepohl, K.H. Distribution of the elements in some major units of the Earth's crust. *GSA Bull.* **1961**, *72*, 175–192. [CrossRef]
39. Kamber, B.S.; Webb, G.E. Transition metal abundances in microbial carbonate: A pilot study based on in situ LA-ICP-MS analysis. *Geobiology* **2007**, *5*, 375–389. [CrossRef]
40. Wedepohl, K.H. The composition of the continental crust. *Geochim. Cosmochim. Acta* **1995**, *59*, 1217–1232. [CrossRef]
41. Taylor, S.R.; McLennan, S.M. The geochemical evolution of the continental crust. *Rev. Geophys.* **1995**, *33*, 241–265. [CrossRef]
42. Bau, M.; Möller, P. Rare earth element systematics of the chemically precipitated component in Early Precambrian iron-formations. *Geochim. Cosmochim. Acta* **1993**, *57*, 2239–2249. [CrossRef]
43. Wood, S.A. The aqueous geochemistry of the rare-earth elements and yttrium: 1. Review of available low-temperature data for inorganic complexes and the inorganic REE speciation of natural waters. *Chem. Geol.* **1990**, *82*, 159–186. [CrossRef]
44. Webb, G.E.; Kamber, B.S. Trace element geochemistry as a tool for interpreting stromatolites. In *Earliest Life on Earth: Habitats, Environments and Methods of Detection*; Golding, S.D., Glikson, M., Eds.; Springer: Dordrecht, The Netherlands, 2011; pp. 127–170. [CrossRef]
45. Bau, M. Controls on the fractionation of isovalent trace elements in magmatic and aqueous systems: Evidence from Y/Ho, Zr/Hf, and lanthanide tetrad effect. *Contrib. Mineral. Petrol.* **1996**, *123*, 323–333. [CrossRef]

46. Censi, P.; Sprovieri, M.; Larocca, D.; Aricò, P.; Saiano, F.; Mazzola, S.; Ferla, P. Alteration effects of volcanic ash in seawater: Anomalous Y/Ho ratios in coastal waters of Central Mediterranean Sea. *Geochim. Cosmochim. Acta* **2007**, *71*, 5405–5422. [CrossRef]
47. Webb, G.E.; Kamber, B.S. Rare earth elements in Holocene reefal microbialites: A new shallow seawater proxy. *Geochim. Cosmochim. Acta* **2000**, *64*, 1557–1565. [CrossRef]

Disclaimer/Publisher's Note: The statements, opinions and data contained in all publications are solely those of the individual author(s) and contributor(s) and not of MDPI and/or the editor(s). MDPI and/or the editor(s) disclaim responsibility for any injury to people or property resulting from any ideas, methods, instructions or products referred to in the content.